ACS NANO

www.acsnano.org

ARTICLE

Energetic Disorder in Doped P3HT: A Crucial Factor in Overcoming Coulomb Binding for Free Charge Generation

Seong Hyeon Kim, Seonghyeon Kang, Minyoung Jeong, Jisang Park, Seungwon Jeong, Hyunji Lee, Chang Yun Son, and Kilwon Cho*

Cite This: https://doi.org/10.1021/acsnano.5c04666

Read Online

ACCESS | Metrics & More | Article Recommendations | Supporting Information

ABSTRACT: Doping of conjugated polymers, which offers precise control over energy levels and electrical conductivity, has faced setbacks because of its low doping efficiency. The majority of generated charge carriers become bound to dopant counterions through Coulomb interaction, leaving only a small fraction of free charges. Although the inherent energetic disorder in polymers may reduce the theoretically predicted Coulomb potential barrier and facilitate the release of bound charges to become mobile, this hypothesis has not been thoroughly quantified. In the present study, we investigate how the energetic disorder of conjugated polymers influences the release of free charges by reducing the activation energy, thus quantitatively assessing the effect of disorder on doping efficiency. Specifically, we examine the relationship between energetic disorder resulting from modifications of the crystallinity of poly(3-hexylthiophene-2,5-diyl) (P3HT) films, a model conjugated polymer, and the quantity of free charge and doping efficiency. A regiorandom P3HT film, characterized by low crystallinity and high static energetic disorder, exhibits an increased concentration of free charges. Consequently, its doping efficiency—defined as the ratio of free charges to total charges—is enhanced. We expect our findings to guide molecular design strategies and materials selection for the development of highly conductive doped-polymer materials.

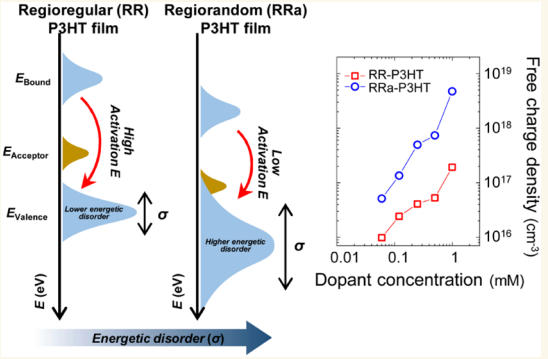

KEYWORDS: *conjugated polymers, energetic disorder, Coulomb binding, free charges, doping efficiency*

INTRODUCTION

Doping of conjugated polymers holds promise as a fundamental technology for next-generation electronic and optical devices such as organic thermoelectric generators and organic photovoltaics because of its ability to precisely tune electrical characteristics.[1−3] In particular, the potential of doping technology for conjugated polymers has been further highlighted by recent achievements demonstrating electrical conductivities exceeding 1000 S cm^{-1} and ZT values above 0.4 in both p-type[4,5] and n-type[6,7] thermoelectric materials, which are widely recognized as one of the most promising applications of the doping approach.[8] Several doping mechanisms of organic semiconductors have been proposed, including a charge transfer process, proton (hydride)-related process, and a Lewis acid−base reaction process, depending on the chemical reactions involved.[9−11] Initially, the charge transfer mechanism was proposed, in which electrons are transferred to lower energy states as a result of the energy level disparity between the dopant and the host material, with fluorinated tetracyanoquinodimethane (TCNQ) compounds serving as representative dopants.[12] Recently, a doping mechanism of conjugated polymers by Lewis acids has been introduced, involving a Lewis acid dopant—such as tris-(pentafluorophenyl)borane (BCF)—which forms an adduct with atmospheric water molecules and facilitates doping via proton transfer followed by electron transfer.[13] Once charge transfer occurs between the conjugated polymer and the dopant, Coulomb forces act between the generated charge and the dopant counterion. The intensity of the binding energy is calculated to be approximately 0.5 eV using the basic electrostatic model $E_b(r) = e^2/(4\pi\varepsilon_0\varepsilon_r r)$, where the dielectric

Received: March 18, 2025
Revised: July 26, 2025
Accepted: July 28, 2025

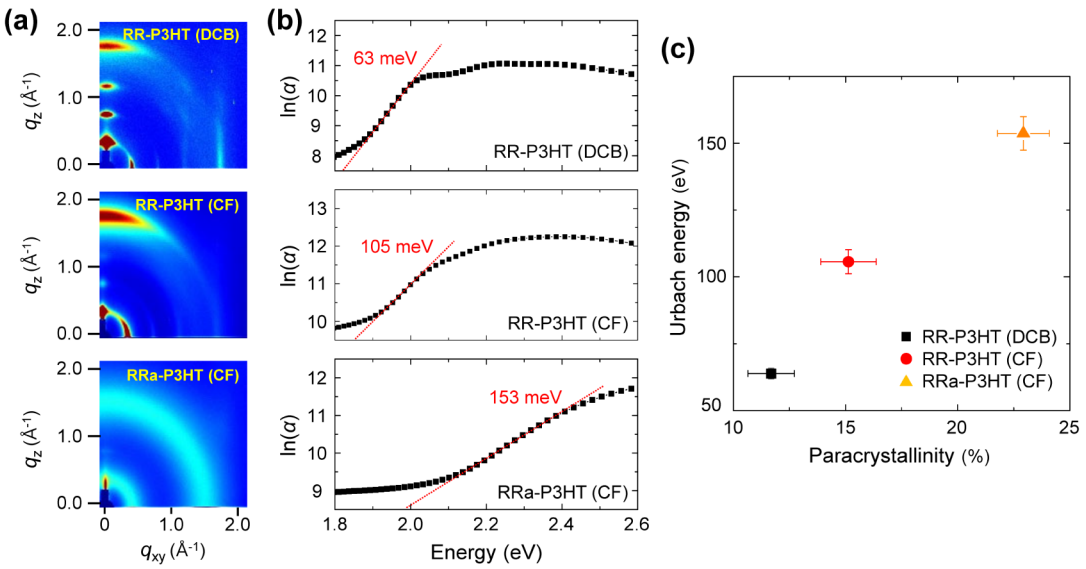

Figure 1. (a) 2D GIWAXS (2D grazing-incidence wide-angle X-ray scattering) images of undoped P3HT films according to regioregularity and used solvents. (b) Absorption coefficient (α) as a function of absorbed photon energy for Urbach energy (E_U) extraction. (c) Correlation between Urbach energy and paracrystallinity in P3HT films, which exhibit different degrees of crystallinity.

constant ε_r = 3 and the intermolecular distance r = 1 nm.[14] The Coulomb binding energy (~0.5 eV) is substantially greater than the thermal energy at room temperature (~26 meV), indicating that the majority of charges generated by doping are trapped in the Coulomb potential and cannot be released as free charge carriers.[15] Despite the theoretical prediction, experimental instances demonstrating electrical conductivity greater than 1000 S cm^{-1} suggest the presence of an underlying mechanism that surpasses the theoretical prediction of an extremely low level of free charges, thereby enhancing doping efficiency.[4,6] An effective strategy to reduce Coulomb interactions and facilitate the generation of free charges involves increasing the spatial separation between the charge and its counterion. This can be accomplished not only by modifying the polymer structure—such as extending side chains or altering the backbone to position the dopant further from the core[16,17] but also by designing dopant molecules with bulky groups around the charge-accepting core, thereby increasing steric shielding.[18−20] In addition, the Coulomb potential overlap,[21] the entropy contribution,[22] and the energetic disorder of conjugated polymers[23] have been suggested as possible scenarios that diminish the Coulomb binding energy between charges and dopant counterions, thereby facilitating the release of free charge carriers from the potential well.

Among these possibilities, the energetic disorder of conjugated polymers, defined as the width of the density of states (DOS), is an inherent factor arising not only from imperfections in the solid-state structure of the polymer but also from thermal fluctuations of intermolecular sites.[24,25] The soft van der Waals bonding nature of organic semiconductors is accompanied by notable dynamic and static energetic disorder.[26−29] Identifying its influence on the doping efficiency is critical for achieving further advancements in doping technology within this field. Leo and coworkers proposed a two-step doping model, which suggests that the activation energy required for charges to release from a bound state to a free charge decreases with increasing energetic disorder of organic molecules.[23] This model is currently used in numerous organic molecular semiconductor doping systems because it effectively elucidates the differences observed between absorption spectra and the results of quantitative experiments on free charges.[21,30−34] However, previous studies on the effect of energetic disorder on free charge formation have primarily focused on small molecules. Furthermore, it has been experimentally shown that the release of free charges stage following the integer charge transfer stage between dopant and host is temperature-dependent. This finding is supported by theoretical analysis based on classical semiconductor statistical equations and advanced computer simulations using molecular dynamics (MD) and density functional theory (DFT). Despite these advances, an experimental relationship between changes in the energetic disorder of conjugated polymers and variations in the amount of free charge released as well as differences in doping efficiency has not been established quantitatively. In other words, in the case of conjugated polymers, where the effect of static energetic disorder is more prominent than in small molecular organic semiconductors investigated in the previous literatures,[23] the relationship between the energetic disorder and the release of free charges, as well as that between the energetic disorder and the doping efficiency, has not been thoroughly investigated. Salzmann and coworkers investigated the effect of energetic disorder in the host polymer on the doping behavior within a typical *p*-type doping system, namely the P3HT/fluorinated TCNQ combinations.[35] They proposed that although both FTCNQ and TCNQ possess similar and relatively low electron affinities (~4.9 eV) compared to the higher ionization energy of P3HT (~5.2 eV), FTCNQ may improve doping efficiency by inducing a broadening of the HOMO density of states (DOS) in P3HT as a result of FTCNQ's significant dipole moment. However, their study relied on computational predictions of DOS broadening, which were consistent with the experimentally measured doping efficiencies for each dopant rather than directly determining DOS broadening through experimental observation. Establishing a clear, quantitative experimental relationship between energetic disorder and doping efficiency in well-characterized

https://doi.org/10.1021/acsnano.5c04666
ACS Nano XXXX, XXX, XXX−XXX

model conjugated polymers would constitute a meaningful contribution to the research field.

In the present study, we modulated the energetic disorder of films of poly(3-hexylthiophene-2,5-diyl) (P3HT), a model conjugated polymer, by varying their crystallinity and then investigated the effects of energetic disorder on the quantity of free charges and the doping efficiency. Specifically, we quantitatively observed that, with increasing energetic disorder of the P3HT films, the amount of free charges released by doping and the doping efficiency increased concurrently. This observation presents a contradictory scenario in which energetic disorder can lead to an increase in the quantity of free charges at a specific doping level, contrary to the typical phenomenon of energetic disorder negatively affecting charge transport. Consequently, in conjugated polymers, the effects of energetic disorder on doping must be carefully assessed against the conflict between the doping efficiency and transport efficiency. Our findings will prompt a reevaluation of the necessity of accounting for the paradoxical influence of energetic disorder of conjugated polymers on their doping efficiency and charge transport. We hope that our results will suggest avenues for molecular design and materials selection with the aim of developing highly conductive doped conjugated polymers.

RESULTS AND DISCUSSION

Conjugated polymers typically exhibit static disorder stemming from their imperfect crystal structures and the distribution of conformational states in their backbone chains, which leads to an inherent distribution in the DOS tail states.[36] To examine the quantitative correlation between the energetic disorder of the conjugated polymers and the generation of free charges, we chose P3HT as our model polymer and modulated its energetic disorder by adjusting its crystallinity in the film state. For film preparation, regioregular P3HT (RR-P3HT) was dissolved in dichlorobenzene (DCB) and chloroform (CF) solvents, and regiorandom P3HT (RRa-P3HT) was dissolved in CF solvent. We assessed the films' crystalline ordering using 2D grazing-incidence wide-angle X-ray scattering (2D-GIWAXS) measurements (Figure 1a). The RR-P3HT (DCB) film exhibited a distinct edge-on orientation of the polymer backbone chains with respect to the substrate, where the (010) peak of the $\pi-\pi$ stack was observed at $q_{xy} \sim 1.7$ Å^{-1} in the in-plane direction, and the (n00) lamellar peak was observed in the out-of-plane direction. The RR-P3HT (DCB) film demonstrated clear semicrystalline properties. The RR-P3HT (CF) film was less crystalline than the RR-P3HT (DCB) film, with a notable reduction in the orientation of the polymer chains. This lower crystallinity was indicated by the diminished intensity and increased width of the peaks in comparison to the intensity and width of the (010) and (n00) peaks in the 2D-GIWAXS pattern of the RR-P3HT (DCB) film. In the pattern of the RRa-P3HT (CF) film, scattering indicative of crystallinity was absent, with only two isotropic rings detected. This result suggests that the RRa-P3HT (CF) film manifests entirely amorphous characteristics. In summary, in the 2D-GIWAXS patterns of RR-P3HT (DCB), RR-P3HT (CF), and RRa-P3HT (CF) films, the intensity of the (n00) lamellar peak progressively diminished, and the crystal orientation was also disturbed. These observations indicate that a decrease in the regioregularity of P3HT and fast evaporation of the solvent during film formation lead to reduced crystallinity in the resultant P3HT films.[37] The crystallinity of the film samples was quantified by calculating the paracrystallinity (g) for the (010) peak associated with the intermolecular $\pi-\pi$ bond (eq 1):[38]

$$g = \frac{1}{2\pi}\sqrt{\Delta \cdot d_{(010)}} \tag{1}$$

where Δ is the full width at half maximum (FWHM) of the diffraction peak and $d_{(010)}$ is the average $\pi-\pi$ bond length. The paracrystallinity g quantifies the cumulative lattice disorder within an imperfect crystal, defined as the standard deviation of lattice spacing normalized by the mean lattice spacing. Because electronic coupling in the $\pi-\pi$ stacking direction is critical for charge transport in edge-on oriented polymer films, our focus was specifically on g along the $\pi-\pi$ stacking direction.[39] The paracrystallinities of the film samples of RR-P3HT (DCB), RR-P3HT (CF), and RRa-P3HT (CF) were 11.7%, 14.5%, and 24.1%, respectively. With increasing paracrystallinity, the distribution of the $\pi-\pi$ bond distance, $d_{(010)}$, became broader, leading to a reduced crystallinity.

To quantify the degree of energetic disorder, we measured the Urbach energy (E_U) from the absorption spectra at the band edge (Figure 1b).[40] Exponential-dependent absorption was observed near the absorption onset of all film samples, and the Urbach energy could be quantitatively extracted using the following equation (eq 2):

$$\alpha(E) = \alpha_0 \exp\left(\frac{E - E_g}{E_U}\right)(E < E_g) \tag{2}$$

where α_0 is a fitting parameter and E_g is an energy corresponding to the bandgap. An increase in Urbach energy signifies a wider distribution of the band tail, indicating an increase in the energetic disorder. The Urbach energies measured for RR-P3HT (DCB), RR-P3HT (CF), and RRa-P3HT (CF) films were 63, 105, and 153 meV, respectively. From these results, we identified an experimental trend indicating a proportional increase in Urbach energy with increasing paracrystallinity (Figure 1c). These observations suggest that within the static disorder of P3HT, the energetic disorder can be notably influenced by modifying the crystallinity of the film.

The energetic disorder in P3HT films can be modulated by adjusting the regioregularity of the polymer and the solvent's boiling point (Figure 1c). Therefore, the RR-P3HT (CF) and RRa-P3HT (CF) films, which exhibited a distinct difference in energetic disorder, were selected for evaluation of the free charge generation and doping efficiency. It has been reported that, in sequential doping, a face-on orientation of the polymer backbone enhances interactions with dopants and facilitates the formation of charge transfer complexes up to a critical dopant concentration, beyond which the dopant begins to diffuse into the bulk of the film.[41] Since this critical concentration is lower than the doping levels employed in our experiments—which are within the range where bulk doping dominates—the impact of molecular orientation on the doping process is considered to be negligible. To eliminate the influence of the orientation of polymer chains and crystals caused by solvents as much as possible, RR-P3HT (DCB) was excluded from the comparison, which exhibited the most distinct orientation.[37] Cyclic voltammetry (CV) measurements revealed that the RR-P3HT (CF) and RRa-P3HT (CF) films exhibit highest occupied molecular orbital (HOMO) levels of

https://doi.org/10.1021/acsnano.5c04666
ACS Nano XXXX, XXX, XXX−XXX

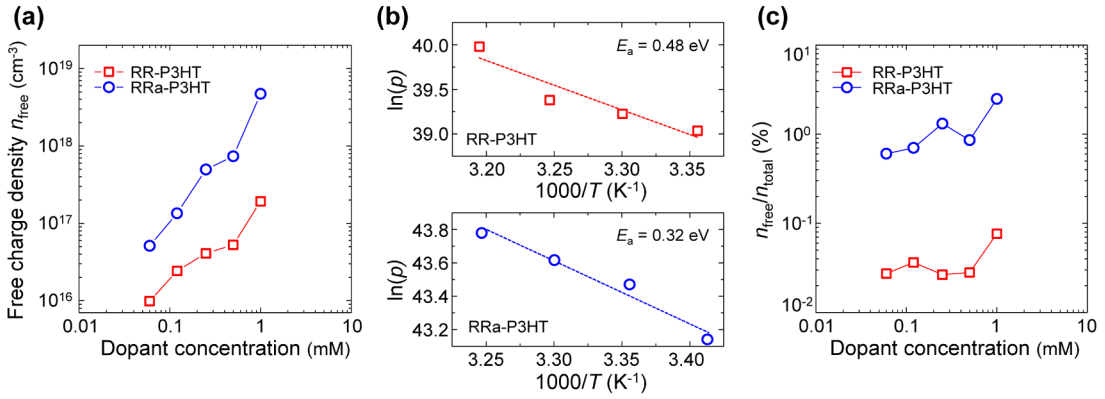

Figure 2. (a) Free charge concentration (n_{free}) in doped RR-P3HT and RRa-P3HT films at low doping levels (0.06 mM ≤ [$FeCl_3$] ≤ 1 mM), measured using Mott−Schottky analysis. (b) Temperature dependence of free charge concentration in doped RR-P3HT and RRa-P3HT films with doping levels at [$FeCl_3$] = 0.06 mM. (c) The ratio of free charge concentration to total charge concentration (n_{free}/n_{total}), indicating doping efficiency. The total carrier concentration used in this context was estimated from the UV−vis−NIR absorption spectra.

−5.27 eV and −5.35 eV, respectively, indicating that RRa-P3HT possesses a deeper HOMO (Figure S1).

In the case of *p*-type doping of P3HT, two distinct doping mechanisms have been identified: integer charge transfer (ICT), where electrons are completely transferred from the polymer host to the dopant, and charge transfer complex (CTC) formation, where hybrid orbitals emerge between the host and dopant, allowing partial electron sharing.[12] While the initial explanation for the dominance of either ICT or CTC focused on the energy alignment between the ionization energy (IE) of P3HT and the electron affinity (EA) of the dopant, subsequent studies have shown that geometric disorder within P3HT also plays a crucial role, leaving ambiguous aspects. It has been reported that higher ICT ratios are associated with increased ordering of P3HT chains and a greater presence of F4TCNQ near the side chain regions, whereas increased CTC ratios correlate with lower main chain ordering.[42,43] Careful consideration of these two doping mechanisms is essential, as they significantly influence both the optical characteristics and the degree of localization of charges within the material. In the present study, a series of experiments was conducted using iron(III) chloride ($FeCl_3$) as a *p*-type dopant that oxidizes both RR-P3HT and RRa-P3HT films effectively, thereby avoiding the coexistence of ICT and CTC species and thereby minimizing the influence of the doping mechanism on the results. Additionally, $FeCl_3$ is capable of doping both the crystalline and amorphous regions of the P3HT films.[44] GIWAXS and AFM analyses confirmed that differences in the crystallinity of RR-P3HT and RRa-P3HT films did not lead to significant variations in the penetration of the dopant into the film (Figures S2−S4).

Mott−Schottky analysis was conducted to measure the free charge generation in the RR-P3HT and RRa-P3HT films (Figure S5). In the Mott−Schottky analysis, charge carriers must be separated from the dopant counterion and diffuse out for a capacitance change to occur in the formed depletion region; thus, only free charges can contribute to this.[23] We measured the free charge concentration at low doping levels (0.06 mM ≤ [$FeCl_3$] ≤ 1 mM), where Mott−Schottky analysis is valid, and discovered that the free charge concentration in the RRa-P3HT films was higher than that in the RR-P3HT films at these low doping levels (Figure 2a). At the lowest doping level ([$FeCl_3$] = 0.06 mM), the RR-P3HT film exhibited a free charge concentration of 9.8 × 10^{15} cm^{-3}, whereas the RRa-P3HT film exhibited a concentration of 5.1 × 10^{16} cm^{-3}. The free charge concentration in both materials increased progressively with increasing doping levels, reaching 1.9 × 10^{17} cm^{-3} and 4.7 × 10^{18} cm^{-3} in the RR-P3HT and RRa-P3HT films, respectively, at [$FeCl_3$] = 1 mM. The RRa-P3HT film, characterized by higher energetic disorder, exhibited higher free charge concentrations than the RR-P3HT film. Notably, at [$FeCl_3$] ≥ 0.25 mM, the free charge concentration in the RRa-P3HT films was more than ten times that in the RR-P3HT films. This observation directly demonstrates that as the energetic disorder (quantified by Urbach energy) of a host polymer increases, the generation of free charges also increases, which aligns with the two-step doping model proposed by Leo and coworkers.[23]

To investigate the origin of the correlation between the energetic disorder of the host polymer and the free charge concentration, we used temperature-dependent Mott−Schottky measurements to calculate the activation energy required for the release of charges (Figure S6). The activation energies for the RR-P3HT and RRa-P3HT films doped with a [$FeCl_3$] = 0.06 mM solution were 0.48 and 0.32 eV, respectively (Figure 2b). This reduction in activation energy for the RRa-P3HT film compared with that for the RR-P3HT film indicates that, in conjugated polymers with a greater degree of energetic disorder, the energy needed to release charges from the bound state around dopant counterions to the valence band decreases (Figure S7).[23,30] Moreover, as the energetic disorder increased, the activation energy in both the RR-P3HT and RRa-P3HT films gradually decreased from the Coulomb binding energy between the dopant counterion and the generated charge, which was predicted to be 0.5 eV using the basic electrostatic model.[14] This decrease in activation energy could lead to more charge carriers being available for electrical conduction than initially speculated. This mechanism, where the energetic disorder of host polymers promotes the release of free charges, might be one of the plausible hypotheses to explain recent experimental results showing high electrical conductivity, for which theoretical predictions based on the basic electrostatic model cannot easily account for.

The total generated charge (n_{total}) was estimated through UV−vis absorption to calculate doping efficiency, independently from the free charges (n_{free}) quantified by Mott−Schottky analysis (Figure S8).[45] This estimation involved converting the absorbance change from the P1 peak, which emerges upon

https://doi.org/10.1021/acsnano.5c04666
ACS Nano XXXX, XXX, XXX−XXX

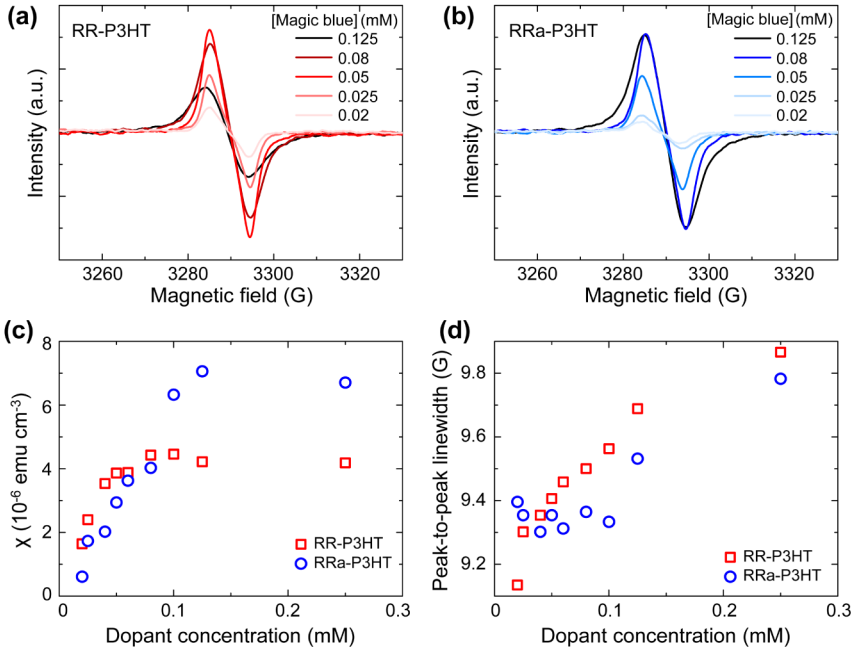

Figure 3. (a,b) ESR (electron spin resonance) spectra of doped RR-P3HT and RRa-P3HT films across a wide range of doping levels (0.01 mM ≤ [magic blue] ≤ 0.25 mM). (c,d) Magnetic susceptibility (χ) and peak-to-peak line width as a function of doping level in RR-P3HT and RRa-P3HT films, derived from ESR spectra in (a,b).

doping, relative to the neutral peak absorbance of the undoped P3HT thin film, on the basis of the Beer–Lambert law.[46] This method entails certain errors, as it requires the exclusion of mutual interference between the two absorption spectra and assumes that the absorbance characteristics of the neutral and ionized segments are similar. Adam J. Moulé and his colleagues addressed these limitations by introducing a correction factor to the conventional approach of calculating charge density based on the relative intensities of neutral and P1 (polaron) absorbance.[47] This allowed them to more accurately determine the ratio of ionized to neutral segments in the conjugated polymer films. However, for the sake of simplicity, we chose not to apply the correction factor in our analysis. The doping efficiency (n_{free}/n_{total}), defined as the ratio of free charge to total generated charge, was notably higher in the RRa-P3HT films, which exhibited high energetic disorder, consistent with experimental results showing a higher free charge concentration in the RRa-P3HT films (Figure 2c). The doping efficiency of the RRa-P3HT films increased from 0.6% to 2.5% as the dopant concentration was varied in the range 0.06 mM ≤ [$FeCl_3$] ≤ 1 mM. In contrast to the RRa-P3HT films, the RR-P3HT films, characterized by their lower energetic disorder, showed an increase in doping efficiency from 0.03% to 0.08% across the same doping levels, yet the doping efficiency remained substantially lower than that of the RRa-P3HT films. This difference was attributed to the difference in the activation energies necessary for the transition of charge from being bound to the dopant counterion to becoming free, highlighting the influence of energetic disorder on the doping efficiency. The notably low doping efficiency observed in this experiment is consistent with predictions in previous studies.[23,48] Despite attempts to maintain a low doping level through sequential doping, the total charge generated, as approximated from the UV–vis–NIR absorption spectra, was ~10^{20} cm^{-3}. This result indicates that a large amount of polarons (~10 mol % relative to the host monomer density) was generated. Hence, this scenario might be indicative of the reserve regime, where the Fermi level is pinned near the acceptor energy level, substantially diminishing the doping efficiency.

We investigated the influence of energetic disorder of host polymers on spin dynamics using electron spin resonance (ESR) measurements, which enable the observation of the spins of generated charges (polarons). In the previous section, $FeCl_3$ was used as a dopant for measuring the doping efficiency. However, because of its tendency to create interference and broaden the peaks in ESR spectra, it was replaced with tris (4-bromophenyl)ammoniumyl hexachloroantimonate (magic blue) for the ESR measurements (Figure 3a,b).[49] After that, the RR-P3HT and RRa-P3HT films were doped to have a wide range of electrical conductivities (Figure S9), both the magnetic susceptibility (χ) and peak-to-peak distance (line width of the ESR signal) were investigated in relation to the doping level (Figure 3c,d). At low doping levels, the spins of the generated charges were assumed to be independent and localized. Consequently, the magnetic susceptibility adheres to Curie's law (eq 3):[50]

$$\chi = \frac{ng^2\mu_B^2 S(S+1)}{3k_B T} \tag{3}$$

where n is the total spin number, g is the spin's g-factor, μ_B is the Bohr magneton, and S is the angular momentum quantum number. In this region, magnetic susceptibility is anticipated to correlate proportionally with the doping level (charge concentration); indeed, both the RR-P3HT and RRa-P3HT films exhibited a linear increase in magnetic susceptibility as a function of the doping level within the low-doping regime (Figure 3c). However, the saturation points in the linear region differed between the two materials: the magnetic susceptibility of the RR-P3HT films reached saturation at a dopant concentration of [magic blue] = 0.06 mM, whereas that of the RRa-P3HT films saturated at a higher dopant concen-

https://doi.org/10.1021/acsnano.5c04666
ACS Nano XXXX, XXX, XXX–XXX

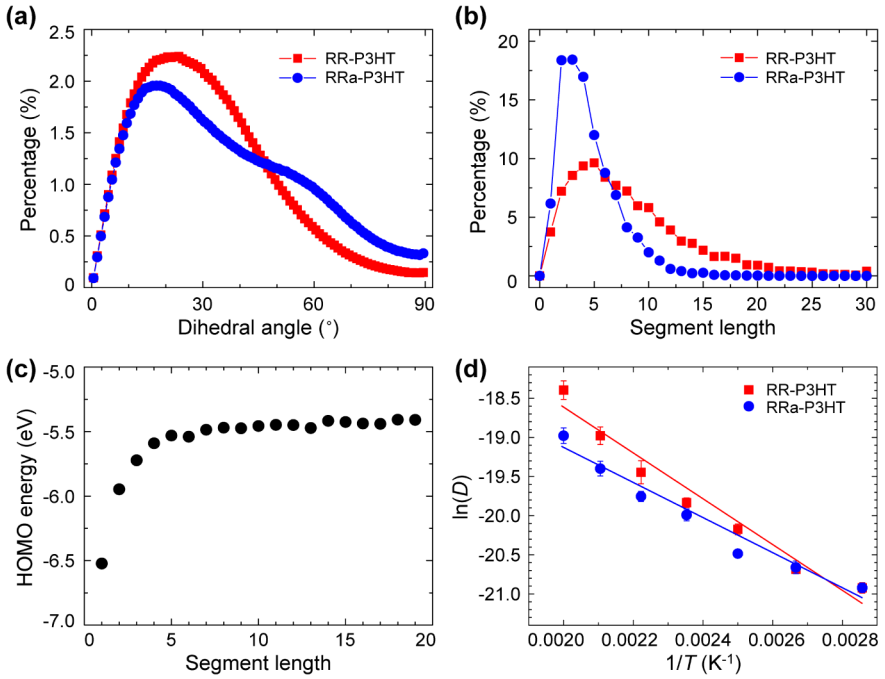

Figure 4. Molecular dynamics (MD) and quantum simulation results of doped RR-P3HT and RRa-P3HT. (a) Polymer backbone dihedral angle distribution of doped RR-P3HT (red) and RRa-P3HT (blue) obtained from long MD simulation. (b) Conjugated segment length characterized following the method by Rühle, Kirkpatrick, and Andrienko.[54] (c) HOMO energies of the P3HT backbone (without side chain) with different conjugated segment length, showing asymptotic convergence to −5.41 eV at long segment length. (d) Temperature dependency of the diffusion coefficient of dopant anions ($FeCl_4^-$). The diffusion coefficients were computed from MD simulation trajectories at various temperatures.

tration of [magic blue] = 0.1 mM. The linear relationship between the magnetic susceptibility of the RRa-P3HT films, characterized by relatively large energetic disorder, and the doping level was substantially more pronounced compared with that of the RR-P3HT films. The observation that the RRa-P3HT films more closely adhered to Curie's law than the RR-P3HT films at that low doping levels suggests that charges generated in a host material with higher energetic disorder are more prone to localization and isolation. Concurrently, while the peak-to-peak distance in the ESR spectra of the RR-P3HT films increased across all doping levels, the peak-to-peak distance in the spectra of the RRa-P3HT films remained constant up to [magic blue] = 0.1 mM, where the magnetic susceptibility reached saturation (Figure 3d). At dopant concentrations beyond [magic blue] = 0.1 mM, the peak-to-peak distance in the spectra of the RRa-P3HT films began to increase. The constant peak-to-peak distance observed in the spectra of the RRa-P3HT films with low doping levels is attributable to the hyperfine interaction with adjacent nuclei, where the ESR peak-to-peak distance is independent of the doping level (charge density).[51,52] Conversely, in the spectra of the RR-P3HT films, which shows a weaker linear relationship between magnetic susceptibility and doping level, the peak-to-peak distance increased consistently across all doping levels; we attributed this tendency to the RR-P3HT films exhibiting a more prominent Elliott−Yafet mechanism than the RRa-P3HT films.[50,53] As a result of spin−orbit coupling, the spin relaxation time is influenced by scattering events involving impurities or phonons, ultimately causing an increase in the peak-to-peak distance of the ESR signal. An inverse relationship exists between the broadening of the peak-to-peak distance and spin relaxation time τ (peak-to-peak distance $\sim \tau^{-1}$). Charge delocalization in the RR-P3HT films was superior to that in the RRa-P3HT films, with the relaxation time decreasing in tandem with the doping levels. These results suggest that the peak-to-peak distance increases as the doping level increase. Conversely, the magnetic susceptibility of the RRa-P3HT films exhibited a marked dependency on the doping level, maintaining a constant peak-to-peak distance at lower doping levels. These results indicate that the charges, influenced by high energetic disorder, remained isolated. The energetic disorder within the RR-P3HT and RRa-P3HT films strongly influences not only the doping efficiency but also the charge localization within the polymer matrix postdoping (Figure S10).

To find the molecular mechanism of the influence of regioregularity of the conducting polymer backbone on the charge localization and charge transport mechanism, we conducted computational analysis combining high-level quantum density functional theory (DFT) calculations and classical molecular dynamics (MD) simulations. These complementary methods enabled us to explain the discrepancy of interaction between each P3HT and dopant anion pair from the perspective of molecular structure and electronic structure. In the MD simulations, we prepared amorphous domains of RR-P3HT and RRa-P3HT films doped with $FeCl_4^-$ anion as a model system. In each of the simulations, a relatively high fraction (0.05) of the polymer backbone was randomly selected to carry a hole charge (+1) and mixed with an equal amount of the counterions. The hole-ion pair-doped polymer systems were equilibrated in an isothermal-isobaric ensemble for 800 ns at various temperatures ranging from 298−500 K and atmospheric pressure. The long simulation time was necessary to reach the density equilibrium of the

https://doi.org/10.1021/acsnano.5c04666
ACS Nano XXXX, XXX, XXX−XXX

polymers at each temperature. An additional 500 ns of production simulations at each temperature were performed in constant volume and temperature to obtain structural and dynamic properties of the equilibrated polymers. These simulations were aimed to mimic the doping environment and describe the interaction between each P3HT film and the dopant, as described in the Methods/Experimental section.

The simulated structures properly captured the structural difference in the two films due to the energetic disorder, where RRa-P3HT showed a broader distribution of the backbone dihedral angle with a higher proportion in the interval of 50° to 90° (Figure 4a). The broader backbone dihedral angle distribution in RRa-P3HT also resulted in a narrower distribution and shortened average of π-conjugation length of the polymer (Figure 4b), characterized by the adjacent torsional angle following Rühle, Kirkpatrick, and Andrienko.[54] The determined conjugation length distribution is able to affect not only morphological differences but also quantum mechanical properties and the thermodynamics of the electron transfer reaction of each segment. To probe this tendency, DFT simulations for the P3HT backbone with different chain lengths and for the $FeCl_3$ dopant were carried out. The HOMO energies of the conjugated polymer backbone (conjugation length >1) were greater than the LUMO energy of $FeCl_3$ (−6.257 eV), following characteristics of type III heterojunctions, with a convergence to −5.41 eV beyond a segment length of six (Figure 4c). Combining with the distribution of segment length and HOMO energies of different segment lengths, we derived the averaged HOMO energy of each P3HT. RR-P3HT presented a higher averaged HOMO energy of −5.57 eV compared to that of RRa-P3HT (−5.70 eV), resulting in a larger energy gap with the $FeCl_3$ LUMO level than RRa-P3HT (Figure S20). Estimated energy differences of 0.687 eV for RR-P3HT and 0.554 eV for RRa-P3HT are in quantitative agreement with the cyclic voltammetry (Figure S1) and UV−vis−NIR absorption spectra (Figure S8) experiments.

Analyzing the temperature (T)-dependent diffusion coefficients (D) of $FeCl_4^-$ anion calculated from MD simulations at 350 K−500 K revealed that the diffusional activation energy (E_a), estimated with an Arrhenius-type relation (eq 4), has a strong correlation with the energetic disorder (Figure 4d).

$$D = D_0 \cdot \exp\left(-\frac{E_a}{RT}\right) \tag{4}$$

Here, D_0 is the asymptotic diffusion coefficient at an infinite temperature limit, and R is the ideal gas constant. The calculated activation barrier of dopant anion diffusion was lower in RRa-P3HT, with a value of 0.606 eV per single anion, compared to the value of 0.782 eV per single anion for RR-P3HT. The difference in activation energies of 0.176 eV is consistent with the temperature-dependent Mott−Schottky analysis (Figure 2b). The reduced diffusional activation energy in RRa-P3HT can be associated with its higher energetic disorder. Since both of the systems were simulated in the amorphous film state, there is little structural difference in the local hole-dopant ion distance distribution. However, due to the lower regioregularity of RRa-P3HT, the P3HT polymer cannot be packed tightly and aligned easily, resulting in the equilibrium density of RR-P3HT (Figure S18) being consistently 1% higher than RRa-P3HT (Figure S19). The larger free volume in RRa-P3HT allows the structural fluctuations of the polymeric backbone and relaxation of hole-paired dopant anions, lowering the diffusional activation energy and increasing energetic disorder. This is in accordance with the crystallinity of RR-P3HT and RRa-P3HT given in the 2D-GIWAXS measurement (Figure 1). Interestingly, the absolute anionic diffusion coefficient at high temperature is higher in RR-P3HT than in RRa-P3HT, in contrast to the greater diffusional activation barrier in RR-P3HT (Figure 4d). This conflicting tendency in the degree of ion transport vs activation barrier is similar to the conflict in the electrical conductivity vs activation barrier of free charge generation observed in experiment. Based on the simulated structural and dynamic properties of the hole-dopant anion pair, we attribute that the higher energetic disorder in RRa-P3HT promotes local relaxation of the polymeric backbone and associated dopant anion, resulting in the reduced activation barrier of both free charge carrier generation and local dopant anion movement. On the other hand, with increased crystallinity and regioregularity, RR-P3HT exhibits faster long-range ion/electron transport at high temperature owing to the longer conjugation segment length and regular ion transport pathway. These computational analyses provide molecular insights for the complex dual role of energetic disorder in the doped P3HT films, providing a promising design route to tailor-made electrical properties of the conjugated films. These results led to the paradoxical conclusion that although the RRa-P3HT films, which exhibit high energetic disorder, are advantageous for the release of free charges, they are clearly disadvantageous for charge transport because of the localization of mobile charge carriers (Figures S11 and S12). In other words, the energetic disorder of host polymers simultaneously affects both the delocalization ratio of doping-induced charges and the delocalization range of carriers, with the ratio and range of delocalized charges having a trade-off relationship (Figure 5). Therefore, a comprehensive consideration of these effects from both perspectives (charge generation and charge transport) is critical for achieving optimized electrical conductivity via doping. Our study was limited to P3HT/$FeCl_3$, which does not suffice to provide generalized information. Further systematic and comprehensive investigations involving various conjugated polymers and dopant combinations could yield valuable insights into this field.

CONCLUSIONS

We quantitatively explored how energetic disorder, a characteristic trait of conjugated polymers, influences the generation of free charges, doping efficiency, and charge localization. By changing the regioregularity of P3HT and selecting different solvents, we modified the crystallinity and, consequently, the extent of static energetic disorder in P3HT films. We observed that an increase in energetic disorder (RR-P3HT (CF) < RRa-P3HT (CF)) led to a higher fraction of free charges that could be released from the Coulomb binding of the dopant's counterion at a given doping level. By measuring the activation energy required for charges to overcome the Coulomb binding, we found an explicit reduction in activation energy for the RRa-P3HT films (0.32 eV), which exhibit higher energetic disorder, compared with that for the RR-P3HT films (0.48 eV). These results support the two-step doping theory, suggesting that, although most charges generated by doping are bound to the dopant's counterion, only a subset becomes active as free charges in conjugated polymers. In addition, our investigation of spin dynamics through ESR measurements

https://doi.org/10.1021/acsnano.5c04666
ACS Nano XXXX, XXX, XXX−XXX

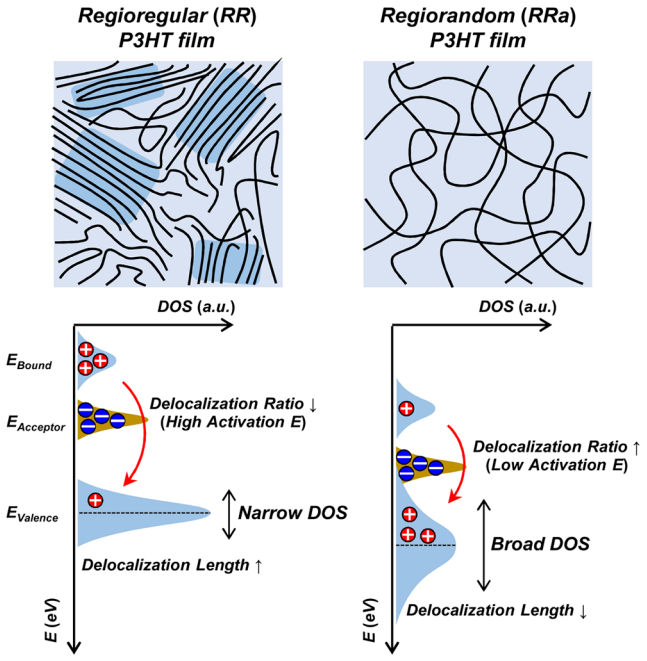

Figure 5. Schematic illustration of the effects of energetic disorder on both the delocalization ratio and delocalization length for charges in *p*-type doped P3HT. In *p*-type doping, holes serve as the majority charge carriers, and the energy axis (*y* axis) is defined for holes. As the crystallinity of the P3HT film decreases, the DOS broadens and exhibits high energetic disorder. This highly energetic disorder promotes the activation of free charges, which increases the delocalization ratio but reduces the delocalization length simultaneously.

indicated charge localization in the RRa-P3HT films, which exhibit greater energetic disorder than the RR-P3HT films, representing a remarkable hopping transport mechanism between isolated states. The energetic disorder of conjugated polymers influences both the delocalization ratio of doping-induced charges and the delocalization range of carriers, creating a trade-off relationship between the ratio and range of delocalized charges. Our findings present a conflicting view of the effect of energetic disorder on doping efficiency and charge transport, underscoring the need for a strategic balance to enhance overall electrical conductivity. Our quantitative analysis of the doping efficiency in P3HT films has a limitation in that it was conducted only at low doping levels, where the Mott–Schottky methodology was applicable (free carrier density $\leq 10^{18}$ cm^{-3}). However, at the high doping levels relevant for practical applications, such as thermoelectric materials, a significantly more complex scenario arises. This includes potential alterations in the polymer microstructure due to excess dopants and the growing influence of carrier–carrier Coulomb interactions, in addition to the dopant–carrier interactions. These complexities suggest that a different aspect of doping efficiency may emerge in the heavily doped regime, necessitating further in-depth investigation beyond the scope of our current study.

METHODS/EXPERIMENTAL

Materials. Both regioregular and regiorandom poly(3-hexylthiophene-2,5-diyl) (P3HT) were purchased from Sigma-Aldrich. The *p*-type dopants, iron(III) chloride ($FeCl_3$) and tris(4-bromophenyl)-ammoniumyl hexachloroantimonate (also known as magic blue), were also purchased from Sigma-Aldrich. Chloroform (CF) and 1,2-dichlorobenzene (DCB) served as solvents for the P3HT polymer, while acetonitrile (ACN) was used as a solvent for the dopants. All solvents were purchased from Sigma-Aldrich.

Doping Reaction and Fabrication of Polymer Films. Regioregular P3HT (RR-P3HT) and regiorandom P3HT (RRa-P3HT) were dissolved in CF or DCB solvent at a concentration of 10 mg mL^{-1}. The dissolved P3HT solutions were stirred in a nitrogen environment for more than 12 h (50 °C for CF, 120 °C for DCB), then spin-coated onto a substrate (1500 rpm, 50 s). The dopant was introduced to the preformed polymer thin films through a solution sequential method, with the doping level being controlled by varying the concentration of the dopant solution (0.06 mM $\leq$ [$FeCl_3$] $\leq$ 40 mM, 0.02 mM $\leq$ [magic blue] $\leq$ 0.25 mM). Following a 60 s reaction of the dopant solution on the polymer thin film, it was removed by vigorous spin coating (4500 rpm for 30 s). The thickness of the P3HT/dopant films ranged from 50 to 60 nm.

Cyclic Voltammetry (CV) Measurement. Cyclic voltammetry (CV) was performed by using the PowerLab/LD system with a scan rate of 50 mV s^{-1}. The conventional three-electrode configuration included a glassy carbon disk electrode coated with a polymer thin film (working electrode), a platinum wire (counter electrode), and a silver wire (reference electrode). An Ag/AgCl electrode served as the reference, and the potential was internally calibrated by using the ferrocenium/ferrocene (Fc^+/Fc^0) redox couple. All measurements were conducted on polymer thin films.

Mott–Schottky Analysis. For Mott–Schottky analysis, we spin-cast P3HT films onto indium tin oxide (ITO) substrates and doped those films with the $FeCl_3$ dopant. Subsequently, 100 nm-thick Al electrodes were thermally evaporated onto the active layer, creating a device with a working area of 5.6 mm^2. Measurements involved sweeping the DC voltage from −0.5 to 0.5 V, with an AC voltage of 20 mV, and controlling the frequency between 1 kHz and 5 kHz, where the phase angle was approximately −90°. These measurements were conducted in a nitrogen-filled glovebox. The carrier density (N_A) was determined from the slope of the linear relationship between C^{-2} and V (eq 5),

$$\frac{\mathrm{d}}{\mathrm{d}V}\left(\frac{1}{C^2}\right) = \frac{2}{q\varepsilon_0\varepsilon_r A^2}\cdot\frac{1}{N_A} \tag{5}$$

where q is the elementary charge, ε_0 is the vacuum permittivity, ε_r is the relative permittivity, and A is the working area in the device.

ESR Measurement. Electron spin resonance (ESR) spectra were acquired at room temperature using JES-FA100 (JEOL) equipment. For the ESR measurements, P3HT films were spin-coated onto a PET substrate and subsequently doped with the magic blue dopant. Spin susceptibilities were determined through the double integration of the ESR spectra, calibrated against a reference powder sample of CuSO4·5H2O obtained from Sigma-Aldrich.

Spectroscopic Analysis. Ultraviolet/visible/near-infrared (UV/vis/NIR) absorption spectroscopy was conducted using a V-770 spectrometer (Jasco), capturing absorption spectra for film samples across the wavelength range of 400–2500 nm at 1 nm intervals. Fourier transform infrared spectroscopy (FT-IR) was carried out on a Vertex 70v (Bruker) in transmittance mode, with spectra obtained over a wavenumber range of 500 cm^{-1} to 5500 cm^{-1}.

Measurement of Electrical Properties. The sheet resistance, R_s, was measured using the four-probe method (PB100, MSTECH), while the film thickness, t, was measured by using a surface profiler (NanoMap-PS, AEP Technology). Electrical conductivity, σ (S cm^{-1}), was derived from the formula $\sigma = (R_s \times t)^{-1}$, where R_s (Ω $\square^{-1}$) represents the sheet resistance and t denotes the film thickness. A laboratory-built setup, comprising two Peltier modules to create a temperature differential and two T-type Cu/constantan thermocouples, was used to concurrently monitor the temperature (Keithley 2400) and Seebeck voltage (Agilent 24700A), from which the Seebeck coefficient, S (μV K^{-1}), was calculated.

https://doi.org/10.1021/acsnano.5c04666
ACS Nano XXXX, XXX, XXX–XXX

ASSOCIATED CONTENT

Supporting Information

The Supporting Information is available free of charge at https://pubs.acs.org/doi/10.1021/acsnano.5c04666.

Experimental details of DFT/MD simulations; CV measurement results and energy levels of used materials; GIWAXS and AFM images of doped P3HT films; Mott−Schottky measurement results; UV−vis−NIR absorption and FT-IR spectra of doped P3HT films; measured and calculated transport properties of doped P3HT films; environmental stability of doped P3HT films (PDF)

AUTHOR INFORMATION

Corresponding Author

Kilwon Cho − *Department of Chemical Engineering, Pohang University of Science and Technology, Pohang 37673, Republic of Korea;* orcid.org/0000-0003-0321-3629; Email: kwcho@postech.ac.kr

Authors

Seong Hyeon Kim − *Department of Chemical Engineering, Pohang University of Science and Technology, Pohang 37673, Republic of Korea*

Seonghyeon Kang − *Department of Chemistry, Seoul National University, Seoul 08828, Republic of Korea*

Minyoung Jeong − *Department of Chemical Engineering, Pohang University of Science and Technology, Pohang 37673, Republic of Korea*

Jisang Park − *Department of Chemical Engineering, Pohang University of Science and Technology, Pohang 37673, Republic of Korea*

Seungwon Jeong − *Department of Chemistry, Pohang University of Science and Technology, Pohang 37673, Korea*

Hyunji Lee − *Department of Chemical Engineering, Pohang University of Science and Technology, Pohang 37673, Republic of Korea*

Chang Yun Son − *Department of Chemistry, Seoul National University, Seoul 08828, Republic of Korea;* orcid.org/0000-0002-0784-6565

Complete contact information is available at: https://pubs.acs.org/10.1021/acsnano.5c04666

Notes

The authors declare no competing financial interest.

ACKNOWLEDGMENTS

This work was supported by the Development of Next-Generation Material of the Korea Planning & Evaluation Institute of Industrial Technology (KEIT), Ministry of Trade, Industry and Energy (MOTIE), Republic of Korea (Project No.: RS-2025-02413058).This work was supported by the National Research Foundation of Korea (NRF) grant (RS-2024-00406548) funded by the Ministry of Science and ICT, Korea. Grazing-incidence wide-angle X-ray scattering (GI-WAXS) measurement was conducted at the 3C and 9A beamlines of the Pohang Accelerator Laboratory (PAL), South Korea.

REFERENCES

(1) Tang, J.; Pai, Y.-H.; Liang, Z. Strategic Insights into Semiconducting Polymer Thermoelectrics by Leveraging Molecular Structures and Chemical Doping. *ACS Energy Lett.* **2022**, *7* (12), 4299−4324.

(2) Dai, Y.; Hu, H.; Wang, M.; Xu, J.; Wang, S. Stretchable transistors and functional circuits for human-integrated electronics. *Nat. Electron.* **2021**, *4* (1), 17−29.

(3) Xu, X.; Feng, K.; Yu, L.; Yan, H.; Li, R.; Peng, Q. Highly Efficient All-Polymer Solar Cells Enabled by p-Doping of the Polymer Donor. *ACS Energy Lett.* **2020**, *5* (7), 2434−2443.

(4) Jacobs, I. E.; Lin, Y.; Huang, Y.; Ren, X.; Simatos, D.; Chen, C.; Tjhe, D.; Statz, M.; Lai, L.; Finn, P. A.; et al. High-Efficiency Ion-Exchange Doping of Conducting Polymers. *Adv. Mater.* **2022**, *34*, No. e2102988.

(5) Kim, G. H.; Shao, L.; Zhang, K.; Pipe, K. P. Engineered doping of organic semiconductors for enhanced thermoelectric efficiency. *Nat. Mater.* **2013**, *12* (8), 719−723.

(6) Tang, H.; Liang, Y.; Liu, C.; Hu, Z.; Deng, Y.; Guo, H.; Yu, Z.; Song, A.; Zhao, H.; Zhao, D.; et al. A solution-processed n-type conducting polymer with ultrahigh conductivity. *Nature* **2022**, *611* (7935), 271−277.

(7) Ma, M.; Ye, G.; Jang, S.; Kuang, Y.; Zhang, L.; Shao, S.; Koster, L. J. A.; Baran, D.; Liu, J. Realizing an N-Type Organic Thermoelectric ZT of 0.46. *ACS Energy Lett.* **2025**, *10* (4), 1813−1820.

(8) Liu, J.; Craighero, M.; Gupta, V. K.; Scheunemann, D.; Paleti, S. H. K.; Järsvall, E.; Kim, Y.; Xu, K.; Reparaz, J. S.; Koster, L. J. A.; et al. Electrically Programmed Doping Gradients Optimize the Thermoelectric Power Factor of a Conjugated Polymer. *Adv. Funct. Mater.* **2024**, *34* (18), 2312549.

(9) Salzmann, I.; Heimel, G.; Oehzelt, M.; Winkler, S.; Koch, N. Molecular Electrical Doping of Organic Semiconductors: Fundamental Mechanisms and Emerging Dopant Design Rules. *Acc. Chem. Res.* **2016**, *49* (3), 370−378.

(10) Zeng, Y.; Zheng, W.; Guo, Y.; Han, G.; Yi, Y. Doping mechanisms of N-DMBI-H for organic thermoelectrics: hydrogen removal vs. hydride transfer. *J. Mater. Chem. A* **2020**, *8* (17), 8323−8328.

(11) Kim, J.; Ju, D.; Kim, S.; Cho, K. Disorder-Controlled Efficient Doping of Conjugated Polymers for High-Performance Organic Thermoelectrics. *Adv. Funct. Mater.* **2024**, *34* (6), 2309156.

(12) Mendez, H.; Heimel, G.; Winkler, S.; Frisch, J.; Opitz, A.; Sauer, K.; Wegner, B.; Oehzelt, M.; Rothel, C.; Duhm, S.; et al. Charge-transfer crystallites as molecular electrical dopants. *Nat. Commun.* **2015**, *6*, 8560.

(13) Yurash, B.; Cao, D. X.; Brus, V. V.; Leifert, D.; Wang, M.; Dixon, A.; Seifrid, M.; Mansour, A. E.; Lungwitz, D.; Liu, T.; et al. Towards understanding the doping mechanism of organic semiconductors by Lewis acids. *Nat. Mater.* **2019**, *18* (12), 1327−1334.

(14) Scaccabarozzi, A. D.; Basu, A.; Anies, F.; Liu, J.; Zapata-Arteaga, O.; Warren, R.; Firdaus, Y.; Nugraha, M. I.; Lin, Y.; Campoy-Quiles, M.; et al. Doping Approaches for Organic Semiconductors. *Chem. Rev.* **2022**, *122* (4), 4420−4492.

(15) Ju, D.; Kim, D.; Yook, H.; Han, J. W.; Cho, K. Controlling Electrostatic Interaction in PEDOT: PSS to Overcome Thermoelectric Tradeoff Relation. *Adv. Funct. Mater.* **2019**, *29* (46), 1905590.

(16) Liu, J.; Ye, G.; Potgieser, H. G. O.; Koopmans, M.; Sami, S.; Nugraha, M. I.; Villalva, D. R.; Sun, H.; Dong, J.; Yang, X.; et al. Amphipathic Side Chain of a Conjugated Polymer Optimizes Dopant Location toward Efficient N-Type Organic Thermoelectrics. *Adv. Mater.* **2021**, *33* (4), No. e2006694.

(17) Liu, J.; Shi, Y.; Dong, J.; Nugraha, M. I.; Qiu, X.; Su, M.; Chiechi, R. C.; Baran, D.; Portale, G.; Guo, X.; et al. Overcoming Coulomb Interaction Improves Free-Charge Generation and Thermoelectric Properties for n-Doped Conjugated Polymers. *ACS Energy Lett.* **2019**, *4* (7), 1556−1564.

(18) Aubry, T. J.; Axtell, J. C.; Basile, V. M.; Winchell, K. J.; Lindemuth, J. R.; Porter, T. M.; Liu, J. Y.; Alexandrova, A. N.; Kubiak, C. P.; Tolbert, S. H.; et al. Dodecaborane-Based Dopants Designed to Shield Anion Electrostatics Lead to Increased Carrier Mobility in a

Doped Conjugated Polymer. *Adv. Mater.* **2019**, *31* (11), No. e1805647.
(19) Charoughchi, S.; Liu, J. T.; Berteau-Rainville, M.; Hase, H.; Askari, M. S.; Bhagat, S.; Forgione, P.; Salzmann, I. Sterically-Hindered Molecular p-Dopants Promote Integer Charge Transfer in Organic Semiconductors. *Angew. Chem., Int. Ed.* **2023**, *62* (31), No. e202304964.
(20) Wu, Y.; Salamat, C. Z.; Leon Ruiz, A.; Simafranca, A. F.; Akmansen-Kalayci, N.; Wu, E. C.; Doud, E.; Mehmedovic, Z.; Lindemuth, J. R.; Phan, M. D.; et al. Using Bulky Dodecaborane-Based Dopants to Produce Mobile Charge Carriers in Amorphous Semiconducting Polymers. *Chem. Mater.* **2024**, *36* (11), 5552−5562.
(21) Mityashin, A.; Olivier, Y.; Van Regemorter, T.; Rolin, C.; Verlaak, S.; Martinelli, N. G.; Beljonne, D.; Cornil, J.; Genoe, J.; Heremans, P. Unraveling the mechanism of molecular doping in organic semiconductors. *Adv. Mater.* **2012**, *24* (12), 1535−1539.
(22) Hood, S. N.; Kassal, I. Entropy and Disorder Enable Charge Separation in Organic Solar Cells. *J. Phys. Chem. Lett.* **2016**, *7* (22), 4495−4500.
(23) Tietze, M. L.; Benduhn, J.; Pahner, P.; Nell, B.; Schwarze, M.; Kleemann, H.; Krammer, M.; Zojer, K.; Vandewal, K.; Leo, K. Elementary steps in electrical doping of organic semiconductors. *Nat. Commun.* **2018**, *9* (1), 1182.
(24) Fratini, S.; Ciuchi, S.; Mayou, D.; de Laissardiere, G. T.; Troisi, A. A map of high-mobility molecular semiconductors. *Nat. Mater.* **2017**, *16* (10), 998−1002.
(25) Kronemeijer, A. J.; Pecunia, V.; Venkateshvaran, D.; Nikolka, M.; Sadhanala, A.; Moriarty, J.; Szumilo, M.; Sirringhaus, H. Two-dimensional carrier distribution in top-gate polymer field-effect transistors: correlation between width of density of localized states and Urbach energy. *Adv. Mater.* **2014**, *26* (5), 728−733.
(26) Fornari, R. P.; Troisi, A. Theory of charge hopping along a disordered polymer chain. *Phys. Chem. Chem. Phys.* **2014**, *16* (21), 9997−10007.
(27) Fratini, S.; Nikolka, M.; Salleo, A.; Schweicher, G.; Sirringhaus, H. Charge transport in high-mobility conjugated polymers and molecular semiconductors. *Nat. Mater.* **2020**, *19* (5), 491−502.
(28) Lu-Díaz, M.; Duhandžić, M.; Harrity, S.; Samanta, S.; Akšamija, Z.; Venkataraman, D. Dopant-Induced Energetic Disorder in Conjugated Polymers: Determinant Roles of Polymer−Dopant Distance and Composite Electronic Structures. *J. Phys. Chem. C* **2024**, *128* (14), 5996−6006.
(29) Ju, D.; Kim, J.; Yook, H.; Han, J. W.; Cho, K. Engineering counter-ion-induced disorder of a highly doped conjugated polymer for high thermoelectric performance. *Nano Energy* **2021**, *90*, 106604.
(30) Schwarze, M.; Gaul, C.; Scholz, R.; Bussolotti, F.; Hofacker, A.; Schellhammer, K. S.; Nell, B.; Naab, B. D.; Bao, Z.; Spoltore, D.; et al. Molecular parameters responsible for thermally activated transport in doped organic semiconductors. *Nat. Mater.* **2019**, *18* (3), 242−248.
(31) Tietze, M. L.; Burtone, L.; Riede, M.; Lüssem, B.; Leo, K. Fermi level shift and doping efficiency inp-doped small molecule organic semiconductors: A photoelectron spectroscopy and theoretical study. *Phys. Rev. B* **2012**, *86* (3), 035320.
(32) Groves, C. Suppression of geminate charge recombination in organic photovoltaic devices with a cascaded energy heterojunction. *Energy Environ. Sci.* **2013**, *6* (5), 1546.
(33) Poelking, C.; Tietze, M.; Elschner, C.; Olthof, S.; Hertel, D.; Baumeier, B.; Wurthner, F.; Meerholz, K.; Leo, K.; Andrienko, D. Impact of mesoscale order on open-circuit voltage in organic solar cells. *Nat. Mater.* **2015**, *14* (4), 434−439.
(34) Albrecht, S.; Vandewal, K.; Tumbleston, J. R.; Fischer, F. S.; Douglas, J. D.; Frechet, J. M.; Ludwigs, S.; Ade, H.; Salleo, A.; Neher, D. On the efficiency of charge transfer state splitting in polymer: fullerene solar cells. *Adv. Mater.* **2014**, *26* (16), 2533−2539.
(35) Hase, H.; Berteau-Rainville, M.; Charoughchi, S.; Orgiu, E.; Salzmann, I. Doping-related broadening of the density of states governs integer-charge transfer in P3HT. *Appl. Phys. Lett.* **2021**, *118* (20), 203301.
(36) Noriega, R.; Rivnay, J.; Vandewal, K.; Koch, F. P.; Stingelin, N.; Smith, P.; Toney, M. F.; Salleo, A. A general relationship between disorder, aggregation and charge transport in conjugated polymers. *Nat. Mater.* **2013**, *12* (11), 1038−1044.
(37) Lee, H.; Lee, D.; Sin, D. H.; Kim, S. W.; Jeong, M. S.; Cho, K. Effect of donor−acceptor molecular orientation on charge photo-generation in organic solar cells. *NPG Asia Mater.* **2018**, *10* (6), 469−481.
(38) Rivnay, J.; Noriega, R.; Kline, R. J.; Salleo, A.; Toney, M. F. Quantitative analysis of lattice disorder and crystallite size in organic semiconductor thin films. *Phys. Rev. B* **2011**, *84* (4), 045203.
(39) Abutaha, A.; Kumar, P.; Yildirim, E.; Shi, W.; Yang, S. W.; Wu, G.; Hippalgaonkar, K. Correlating charge and thermoelectric transport to paracrystallinity in conducting polymers. *Nat. Commun.* **2020**, *11* (1), 1737.
(40) Venkateshvaran, D.; Nikolka, M.; Sadhanala, A.; Lemaur, V.; Zelazny, M.; Kepa, M.; Hurhangee, M.; Kronemeijer, A. J.; Pecunia, V.; Nasrallah, I.; et al. Approaching disorder-free transport in high-mobility conjugated polymers. *Nature* **2014**, *515* (7527), 384−388.
(41) Zhang, F.; Mohammadi, E.; Qu, G.; Dai, X.; Diao, Y. Orientation-Dependent Host-Dopant Interactions for Manipulating Charge Transport in Conjugated Polymers. *Adv. Mater.* **2020**, *32* (39), No. e2002823.
(42) Stanfield, D. A.; Wu, Y.; Tolbert, S. H.; Schwartz, B. J. Controlling the Formation of Charge Transfer Complexes in Chemically Doped Semiconducting Polymers. *Chem. Mater.* **2021**, *33* (7), 2343−2356.
(43) Wu, E. C.; Salamat, C. Z.; Tolbert, S. H.; Schwartz, B. J. Molecular Dynamics Study of the Thermodynamics of Integer Charge Transfer vs Charge-Transfer Complex Formation in Doped Conjugated Polymers. *ACS Appl. Mater. Interfaces* **2022**, *14*, 26988.
(44) Zhong, Y.; Untilova, V.; Muller, D.; Guchait, S.; Kiefer, C.; Herrmann, L.; Zimmermann, N.; Brosset, M.; Heiser, T.; Brinkmann, M. Preferential Location of Dopants in the Amorphous Phase of Oriented Regioregular Poly(3-hexylthiophene-2,5-diyl) Films Helps Reach Charge Conductivities of 3000 S cm−1. *Adv. Funct. Mater.* **2022**, *32* (30), 2202075.
(45) Lim, E.; Peterson, K. A.; Su, G. M.; Chabinyc, M. L. Thermoelectric Properties of Poly(3-hexylthiophene) (P3HT) Doped with 2,3,5,6-Tetrafluoro-7,7,8,8-tetracyanoquinodimethane (F4TCNQ) by Vapor-Phase Infiltration. *Chem. Mater.* **2018**, *30* (3), 998−1010.
(46) Jaglarz, J.; Malek, A.; Sanetra, J. Thermal Dependence of Optical Parameters of Thin Polythiophene Films Blended with PCBM. *Polymers* **2018**, *10* (4), 454.
(47) Moulé, A. J.; Gonel, G.; Murrey, T. L.; Ghosh, R.; Saska, J.; Shevchenko, N. E.; Denti, I.; Fergerson, A. S.; Talbot, R. M.; Yacoub, N. L.; et al. Quantifying Polaron Mole Fractions and Interpreting Spectral Changes in Molecularly Doped Conjugated Polymers. *Adv. Electron. Mater.* **2022**, *8* (4), 2100888.
(48) Tietze, M. L.; Pahner, P.; Schmidt, K.; Leo, K.; Lüssem, B. Doped Organic Semiconductors: Trap-Filling, Impurity Saturation, and Reserve Regimes. *Adv. Funct. Mater.* **2015**, *25* (18), 2701−2707.
(49) Houze, E.; Nechtschein, M.; Pron, A. Fixed-spin-induced ESR linewidth and polaron mobility in conducting polymers. *Phys. Rev. B* **1997**, *56* (19), 12263−12267.
(50) Tanaka, H.; Kanahashi, K.; Takekoshi, N.; Mada, H.; Ito, H.; Shimoi, Y.; Ohta, H.; Takenobu, T. Thermoelectric properties of a semicrystalline polymer doped beyond the insulator-to-metal transition by electrolyte gating. *Sci. Adv.* **2020**, *6*, No. eaay8065.
(51) Tanaka, H.; Nishio, S.; Ito, H.; Kuroda, S.-I. Microscopic signature of insulator-to-metal transition in highly doped semicrystalline conducting polymers in ionic-liquid-gated transistors. *Appl. Phys. Lett.* **2015**, *107* (24), 243302.
(52) Matsui, H.; Kumaki, D.; Takahashi, E.; Takimiya, K.; Tokito, S.; Hasegawa, T. Correlation between interdomain carrier hopping and apparent mobility in polycrystalline organic transistors as investigated by electron spin resonance. *Phys. Rev. B* **2012**, *85* (3), 035308.

https://doi.org/10.1021/acsnano.5c04666
ACS Nano XXXX, XXX, XXX−XXX

(53) Elliott, R. J. Theory of the Effect of Spin-Orbit Coupling on Magnetic Resonance in Some Semiconductors. *Phys. Rev.* **1954**, *96* (2), 266−279.
(54) Ruhle, V.; Kirkpatrick, J.; Andrienko, D. A multiscale description of charge transport in conjugated oligomers. *J. Chem. Phys.* **2010**, *132* (13), 134103.

https://doi.org/10.1021/acsnano.5c04666
ACS Nano XXXX, XXX, XXX−XXX